

Effect of Al₂O₃ on the operation of SiN_x-based MIS RRAMs

A.E. Mavropoulis^a, N. Vasileiadis^{a,b}, P. Normand^a, C. Theodorou^c, G. Ch. Sirakoulis^b, S. Kim^d, P. Dimitrakis^a

^aInstitute of Nanoscience and Nanotechnology, NCSR "Demokritos", Ag. Paraskevi 15341, Greece

^bDepartment of Electrical and Computer Engineering, Democritus University of Thrace, Xanthi 67100, Greece

^cUniv. Grenoble Alpes, Univ. Savoie Mont Blanc, CNRS, Grenoble INP, IMEP-LAHC, 38000 Grenoble, France

^dDivision of Electronics and Electrical Engineering, Dongguk University, Seoul 04620, South Korea

Abstract

The role of a 3 nm Al₂O₃ layer on top of stoichiometric LPCVD SiN_x MIS RRAM cells is investigated by using various electrical characterization techniques. The conductive filament formation is explained, and a compact model is used to fit the current-voltage curves and find its evolution during each operation cycle. The conduction in SiN_x is also studied.

1. Introduction

A large variety of resistive random-access memory (RRAM) technologies are prominent. Nevertheless, a few fulfill the requirements for CMOS integration and meet the commercialization standards. SiN_x, which is widely used for charge-trapping nonvolatile memories in Flash SONOS [1, 2, 3] and Vertical CT-NVMs [4], is found to exhibit competitive resistance switching (RS) properties and attractive SiN_x-based RRAM devices have been recently demonstrated [5, 6, 7] utilizing a metal-insulator-semiconductor structure. These properties render SiN_x as a promising candidate for neuromorphic, in-memory and edge computing [6, 8, 9], as well as for security applications by creating true random number generators [10, 11]. Moreover, Al₂O₃ has been used in the past as a buffer layer in RRAMs to improve the RS and the cycle-to-cycle variations [12]. In this context, we investigated the effect of inserting a thin Alumina layer between the top electrode and SiN_x.

Silicon wafers were implanted with Phosphorous using 60 keV and a dose of $1 \times 10^{15} \text{ cm}^{-2}$ and were then annealed at 950 °C for 20 min in an N₂ environment, creating a heavily doped n⁺⁺ ($N_d = 1 \times 10^{20} / \text{cm}^3$) substrate. A 7 nm LPCVD SiN_x ($x = 1.27$) was deposited on the Silicon wafer. After that a 3 nm Al₂O₃ layer was deposited by MEMS ALD. Finally, the top electrode (TE) was realized using 30 nm Cu and 30 nm Pt to prevent oxidation. The metal contact on the Si bottom electrode (BE) was formed by Al evaporation. A sample without the Al₂O₃, called hereafter reference, was prepared for comparison using the exact same processing steps mentioned previously. The structure of the fabricated devices is presented in the inset of Figure 1a. The DC electrical characterization of the RRAMs is performed using HP4155 and Tektronix 4200A, and the impedance spectroscopy measurements using HP4284 and Zurich Instruments MFIA.

2. Electrical characterization

To start with, current-voltage sweeps were performed using different compliance currents (I_{CC}) during the SET process. The voltage was applied on the TE and the BE was always grounded. Characteristic I-V curves are presented in Figure 1b. The curves of the reference and the Al₂O₃/SiN_x devices are similar in terms of current levels for the HRS and LRS. However, the major difference resides in the SET/RESET voltages, which are significantly higher for the Al₂O₃/SiN_x samples. This is proven by statistically analysing the SET/RESET voltages for both samples (Figure 1c). The standard deviation to mean ratio (σ/μ) is calculated, which is indicative of the variation of these voltages. The addition of Al₂O₃ slightly reduced the high resistance state (HRS) variability. Nevertheless, the low resistance state (LRS) variability increased. It can also be seen that there is a 0.9 V difference in the mean SET voltage between the samples (Table 1), which can be attributed to the voltage drop on the Al₂O₃. By calculating the band diagram (Figure 1c) using the Boise State University Band Diagram Program [13], it is found that the voltage drop on the 3 nm Al₂O₃ layer when +5 V is applied to the top electrode (TE) is 0.9 V, which corresponds exactly to the value derived from the mean SET voltages calculated before. The increased SET voltage indicates that the addition of the Al₂O₃ only added a voltage drop and the resistance switching phenomena take place exclusively inside the SiN_x.

Table 1 Mean SET/RESET voltages and standard deviation.

Sample	V _{SET}			V _{RESET}		
	μ	σ	σ/μ	μ	σ	σ/μ
Al ₂ O ₃ /SiN _x	4.54	0.67	0.15	-4.22	0.43	0.10
Reference	3.61	0.19	0.05	-2.92	0.43	0.15

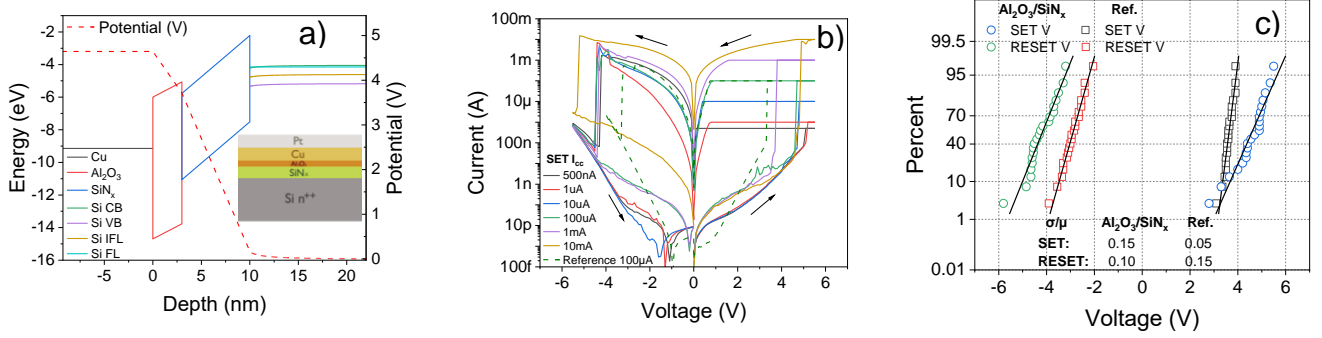


Figure 1 a) Ideal band diagram of $\text{Al}_2\text{O}_3/\text{SiN}_x$ under +5 V bias on the TE (left y axis) and potential across the dielectric (right y axis), b) I-V sweeps with different I_{CC} and c) SET/RESET voltage statistics for the $\text{Al}_2\text{O}_3/\text{SiN}_x$ and reference samples.

After that, multiple SET/RESET cycles were performed using voltage sweeps with the same conditions ($I_{CC} = 100 \mu\text{A}$, 5.5 V for SET and -7 V for RESET) and the current after each SET/RESET operation was measured at 0.5 V. Typically, the samples with Al_2O_3 were able to perform more than 100 cycles, with further improvement for optimization by fine tuning the SET/RESET voltages. Endurance could also be improved by changing the substrate to SOI, where the self-compliance property of the SiN_x memristors has been demonstrated [14]. Furthermore, it should be emphasized that voltage sweep measurements degrade device performance severely compared to pulsed or ramped voltage operation [15]. The memory window evolution, which is the ratio between LRS/HRS, is shown in Figure 2a. Initially, this window is 10^4 and after ~ 20 cycles it stabilizes to 10^5 . This is a similar behavior to the one studied before on the reference sample [16], where the HRS read current decreased in the first 30 cycles. This can be explained by the reduction of the conductive filament gap of the LRS after each cycle. This conductive filament (CF) is formed from traps, specifically Nitrogen vacancies which result in Silicon dangling bonds and allow current to flow through them under electric field [17, 18]. The fact that the CF is created by Nitrogen vacancies means that it is possible to simulate the I-V curves using the compact model of Chen P.-Y [19], which is based on oxygen vacancies in an oxide that act as electron hopping sites. The equation that describes the relationship between current and voltage is:

$$I = I_0 \exp\left(-\frac{g}{g_0}\right) \sinh\left(\frac{V}{V_0}\right) \quad (1)$$

where g is the gap distance between the tip of the CF and the TE and I_0 , g_0 , V_0 are fitting parameters, denoting the current, the gap and the voltage. According to [19], the parameters I_0 , g_0 and V_0 do not have a specific physical meaning and are used to describe the non-linearity of the I-V characteristics. It is found that the I-V curves of our samples fit very well with this model and the evolution of the CF every cycle can be calculated. The CF exponentially decays until cycle 30 as seen in Figure 2b. This means that the model can be successfully used to simulate our devices in circuit level designs. I_0 and g_0 are the same during the fitting of the I-V for every cycle ($I_0 = 25.4 \mu\text{A}$, $g_0 = 0.275\text{nm}$). However, V_0 changes from cycle to cycle, as shown in Figure 2c, without exhibiting any discernable dependence. In addition, the increased LRS variability after 30 cycles (Figure 2a) is mainly attributed to the stochastic number of conductive paths, the stochastic process of ion movement as well as the variation of the gap, g . These processes have stronger impact due to the degradation of the cell's life. The ambient temperature increase will potentially result in higher currents (depending on the conduction mechanism, e.g., Ohmic, Poole-Frenkel, TAT), which will lead to greater variation of the HRS/LRS and the cell endurance will be reduced [20]. The local temperature increase results in higher energy ion movement and thicker filaments during switching. Thus, LRS exhibits greater variation due to the stochastic variation of the gap and is reduced due to the larger diameter of the conductive filaments. Furthermore, LRS can get stuck at a specific value at high temperatures because the kinetic energy of the ions moving towards the TE causes chemical reactions and so, the TE is chemically modified [21, 22].

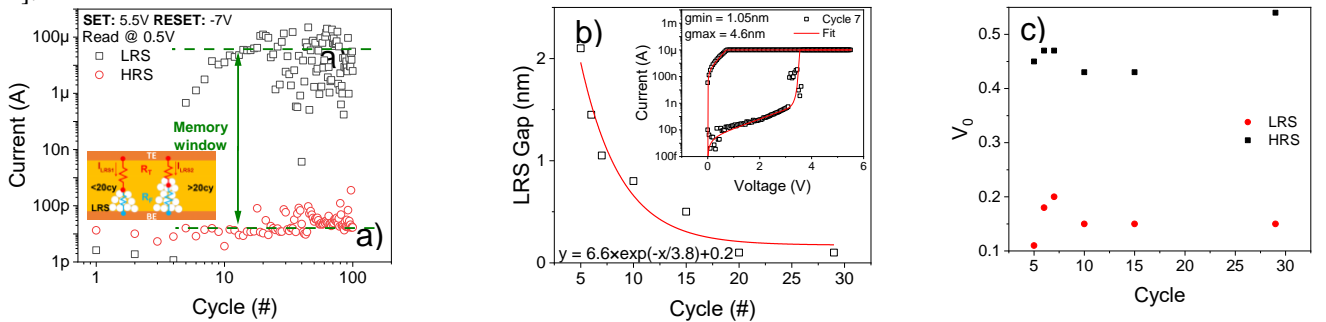


Figure 2 Multiple operation cycles with the same SET/RESET conditions a) HRS/LRS at 0.5 V, b) CF evolution at the first 30 cycles (inset depicts a typical fit in the 7th cycle) and c) V_0 fitting parameter evolution for each cycle.

Moreover, impedance spectroscopy measurements were performed for pristine and cycled devices, i.e., after the SET/RESET sweeps using different SET I_{CC} , utilizing an AC small signal of 25 mV and a DC bias of 0.1 V on the TE. The Nyquist plots for $\text{Al}_2\text{O}_3/\text{SiN}_x$ devices at LRS form a semicircle (Figure 3a) indicative of an equivalent circuit consisting of a resistor (R_p) with a capacitor (C_p) in parallel and a resistor in series (R_s). Physically, R_p and C_p correspond to the resistance of the conductive paths formed during SET and the capacitance of the remaining insulating (no-switched) material region, respectively. R_p decreases with increasing SET I_{CC} (Table 2), resulting in a more conductive CF. The dielectric constant ($\epsilon' = \text{Re}(\epsilon^*) = \epsilon$) was also extracted (Figure

3b) for pristine samples, and it was found to be significantly higher (~7.7) than the reference sample (~5.5), which is expected due to the addition of the 3 nm Al₂O₃, with a reported dielectric constant of 6.7 [23]. Furthermore, the AC conductance (σ') was calculated (Figure 3c) by subtracting the DC part from the measurements and it becomes clear that σ' varies as $\sim f^s$. The values of exponent s range from 1.59 to 1.67 for the LRS and 1.69 for the HRS and denote that the conduction in SiN_x is mainly governed by trap-to-trap tunneling mechanisms (s is close to 2) [24]. The equations

$$\varepsilon(\omega) = \frac{1}{i\omega C_0 Z(\omega)} \quad (2)$$

and

$$\sigma(\omega) = i\omega\varepsilon_0\varepsilon(\omega) \quad (3)$$

were used to calculate the dielectric constant and the conductance for the impedance measurements, where ω the angular frequency, ε_0 the permittivity of free space and C_0 the geometrical capacitance ($C_0 = A\varepsilon_0/d$, d : thickness of the dielectric, A : area of the dielectric) [25].

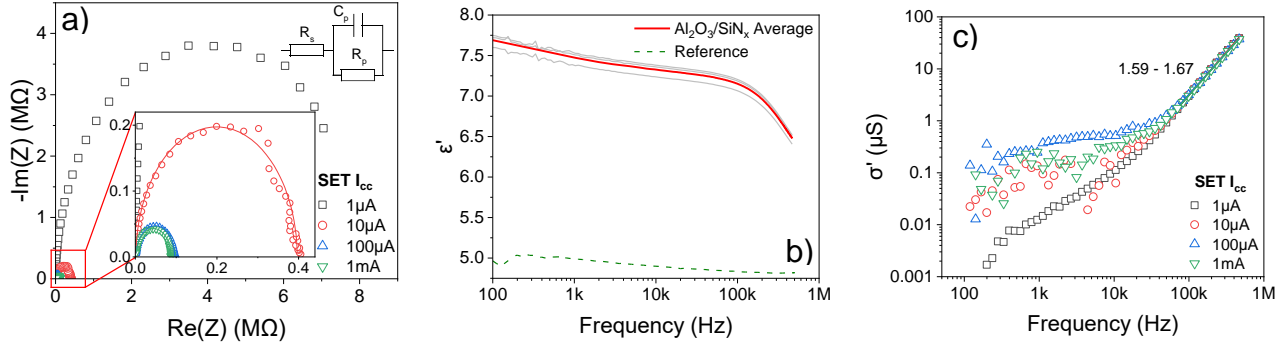


Figure 3 a) Nyquist plots of Al₂O₃/SiN_x devices SET with different I_{cc} , b) dielectric constant of pristine sample and c) AC conductance in the LRS after SET with different I_{cc} .

Table 2 Modelling parameters for Nyquist plots at LRS.

SET I_{cc}	C_p (pF)	R_p (kΩ)
10 μA	62.1	395
100 μA	61.3	94.8
1 mA	61.1	123.5

3. Conclusions

The switching characteristics of memristors with and without Al₂O₃ reveal that the formed filament at LRS is probably due to the formation of nitrogen vacancies and not due to Cu diffusion in the SiN_x. It is concluded that these devices can be SET at different resistance levels by varying the I_{cc} . Moreover, the SET/RESET voltages are higher compared to the reference sample, corresponding to the voltage drop on the Al₂O₃. This device can perform multiple operation cycles, with the memory window increasing in the first twenty, which according to a compact model fit of the I-V curves, is attributed to the decrease of the LRS gap between the CF and the TE. The filamentary conduction at LRS is also proved by the applied model. In addition, impedance spectroscopy measurements revealed that the conduction in SiN_x is mostly governed by trap-to-trap tunneling mechanisms.

Acknowledgements

This work was financially supported by the research project “LIMA-chip” (Proj.No. 2748) of the Hellenic Foundation for Research and Innovation (HFRI).

References

- [1] P. Dimitrakis, "Introduction to NVM Devices.," in *Charge-Trapping Non-Volatile Memories*, P. Dimitrakis, Ed., Springer, Cham, 2015.
- [2] J. Brewer and M. Gill, *Nonvolatile memory technologies with emphasis on Flash*, New York, NY: Wiley, 2008.
- [3] K. Ramkumar, "Charge trapping NVMs with metal oxides in the memory stack," in *Metal Oxides for Non-volatile Memory*, P. Dimitrakis, I. Valov and S. Tappertzhofen, Eds., Elsevier, 2022.
- [4] H. Lue, "3D NAND Flash Architectures," in *Charge-Trapping Non-Volatile Memories*, P. Dimitrakis, Ed., Springer, Cham, 2015.
- [5] N. Vasileiadis, P. Karakolis, P. Mandylas, V. Ioannou-Sougleridis, P. Normand, M. Perego, P. Komninou, V. Ntinis, I.-A. Fyrigos, I. Karafyllidis, G. C. Sirakoulis and P. Dimitrakis, "Understanding the Role of Defects in Silicon Nitride-Based Resistive Switching Memories Through Oxygen Doping," *IEEE Transactions on Nanotechnology*, vol. 20, pp. 356-364, 2021.
- [6] N. Vasileiadis, V. Ntinis, G. C. Sirakoulis and P. Dimitrakis, "In-Memory-Computing Realization with a Photodiode/Memristor Based Vision Sensor," *Materials*, vol. 14, no. 18, p. 5223, 2021.
- [7] N. Vasileiadis, P. Loukas, P. Karakolis, V. Ioannou-Sougleridis, P. Normand, V. Ntinis, I.-A. Fyrigos, I. Karafyllidis, G. C. Sirakoulis and P. Dimitrakis, "Multi-level resistance switching and random telegraph noise analysis of nitride based memristors," *Chaos, Solitons & Fractals*, Vols. 153, Part 1, p. 111533.
- [8] S. Kim, H. Kim, S. Hwang, M. Kim, Y. Chang and B. Park, "Analog synaptic behavior of a silicon nitride memristor," *ACS applied materials & interfaces*,

vol. 9, no. 46, pp. 40420-40427, 2017.

- [9] N. Vasileiadis et al., "A New 1P1R Image Sensor with In-Memory Computing Properties Based on Silicon Nitride Devices," *IEEE International Symposium on Circuits and Systems (ISCAS), Daegu, Korea*, pp. 1-5, 2021.
- [10] N. Vasileiadis, P. Dimitrakis, V. Ntinias and G. C. Sirakoulis, "True Random Number Generator Based on Multi-State Silicon Nitride Memristor Entropy Sources Combination," *International Conference on Electronics, Information, and Communication (ICEIC), Jeju, Korea (South)*, pp. 1-4, 2021.
- [11] R. Carboni and D. Ielmini, "Stochastic Memory Devices for Security and Computing," *Adv. Electron. Mater.*, 2019.
- [12] L. Chen et al., "Highly Uniform Bipolar Resistive Switching With Al₂O₃ Buffer Layer in Robust NbAlO-Based RRAM," *IEEE Electron Device Letters*, vol. 31, no. 4, pp. 356-358, April 2010.
- [13] R. Southwick III* and W. Knowlton, "Stacked Dual Oxide MOS Energy Band Diagram Visual Representation Program," *IRW student paper, Invited Paper, IEEE Transactions on Device and Materials Reliability*, vol. 6, no. 2, p. 136 – 145, 2006. <https://www.boisestate.edu/nano/research-areas/multi-dielectric-energy-band-diagram-program/>
- [14] A. Mavropoulos, N. Vasileiadis, C. Theodorou, L. Sygellou, P. Normand, G. C. Sirakoulis and P. Dimitrakis, "Effect of SOI substrate on silicon nitride resistance switching using MIS structure," *Solid-State Electronics*, vol. 194, 2022.
- [15] G. Sassine, C. Cagli, J. -F. Nodin, G. Molas and E. Nowak, "Novel Computing Method for Short Programming Time and Low Energy Consumption in HfO₂ Based RRAM Arrays," *IEEE Journal of the Electron Devices Society*, vol. 6, pp. 696-702, 2018.
- [16] A. E. Mavropoulos, N. Vasileiadis, P. Normand, V. Ioannou-Sougleridis, K. Tsakalos, G. C. Sirakoulis and P. Dimitrakis, "Synaptic MIS Silicon Nitride Resistance Switching Memory Cells on SOI Substrate," in *2023 IEEE 23rd International Conference on Nanotechnology (NANO)*, Jeju City, Korea, 2023.
- [17] A. Mavropoulos, N. Vasileiadis, C. Bonafos, P. Normand, V. Ioannou-Sougleridis, G. C. Sirakoulis and P. Dimitrakis, "Silicon nitride resistance switching MIS cells doped with silicon atoms," *Solid-State Electronics*, vol. 213, 2024.
- [18] M. Yang, H. Wang, X. Ma, H. Gao and B. Wang, "Effect of nitrogen-accommodation ability of electrodes in SiN_x-based resistive switching devices," *Appl. Phys. Lett.*, vol. 111, no. 23, p. 3510, 2017.
- [19] P. -Y. Chen and S. Yu, "Compact Modeling of RRAM Devices and Its Applications in 1T1R and 1S1R Array Design," *IEEE Transactions on Electron Devices*, vol. 62, no. 12, pp. 4022-4028, Dec. 2015.
- [20] J. Singh and B. Raj, "Temperature dependent analytical modeling and simulations of nanoscale memristor," *Engineering Science and Technology, an International Journal*, vol. 21, no. 5, pp. 862-868, 2018.
- [21] X. Guan, S. Yu and H.-S. P. Wong, "A SPICE Compact Model of Metal Oxide Resistive Switching Memory With Variations," *IEEE Electron Device Letters*, vol. 33, no. 10, pp. 1405-1407, 2012.
- [22] J. Roldán and e. al., "Variability in Resistive Memories," *Adv. Intell. Syst.*, vol. 5, no. 6, 2023.
- [23] M. Groner, J. Elam, F. Fabreguette and S. George, "Electrical characterization of thin Al₂O₃ films grown by atomic layer deposition on silicon and various metal substrates," *Thin Solid Films*, vol. 413, no. 1-2, pp. 186-197, 2002.
- [24] S. Yu, R. Jeyasingh, Y. Wu and H.-S. P. Wong, "AC conductance measurement and analysis of the conduction processes in HfO_x based resistive switching memory," *Appl. Phys. Lett.*, vol. 99, no. 23, p. 232105, 5 December 2011.
- [25] E. Barsoukov and D. J. Ross Macdonald, Eds., *Impedance Spectroscopy: Theory, Experiment, and Applications*, Hoboken, New Jersey: John Wiley & Sons, Inc., 2005.